Modeling the Radar Signature of Raindrops in Aircraft Wake Vortices

Zhongxun Liu *

Institut Superieur de l'Aeronautique et de l'Espace, University of Toulouse, Toulouse, France

Nicolas Jeannin

Department of Electromagntic and Radar, ONERA, Toulouse, France

Francois Vincent

Institut Superieur de l'Aeronautique et de l'Espace, University of Toulouse, Toulouse, France

Xuesong Wang

College of Electronic Science and Engineering, National University of Defense Technology, Changsha, P.R.China

* *Corresponding author address:* Zhongxun Liu, ISAE, 10 Avenue Edouard Belin, Toulouse, France 31400.

E-mail: zhongxun.liu@gmail.com

ABSTRACT

The present work is dedicated to the modeling and evaluation of the radar signature of raindrops within wake vortices. This is achieved through the computation of the motion equation of raindrops within the wake vortex flow. Based on the inhomogeneous distribution of raindrops within wake vortices, the radar echo model is computed for raindrops in a given pulse resolution volume. Simulated Radar Doppler signature of raindrops within wake vortices is illustrated to be a potential criterion for identifying wake vortex hazard in air traffic control. The dependence of the radar signature on various parameters, including the radial resolution, antenna elevation angle, is also analyzed.

1. Introduction

When flying in the atmosphere, an aircraft generates two counter-rotating vortices of strong strength lasting for several minutes. Those wake vortices are hazardous if encountered by other flying aircrafts, especially during take-off and landing phases. Current ICAO (International Civil Aviation Organization) safety separation standard is based on the weight category of the aircrafts, without considering the dynamic evolution of wake vortex. This standard separation is very conservative most of the times but may still enable vortex encounter in some particular weather conditions. Erroneous instructions from flight controllers have ever caused several accidents with the aircrafts entering into the wake vortex of the previous aircraft (Gerz et al. 2002; Proctor et al. 2004). With the great growth of air traffic, an optimal separation scheme based on monitoring wake vortex behavior in real time, can greatly increase the aviation safety, as well as the airport handling capacity which are major commercial issues (Bobylev et al. 2010; Barbaresco and Meier 2010).

The candidate technologies for wake vortex monitoring include Radar, Lidar, and Sodar (Rubin 2000; Barbaresco et al. 2007; Holzpfel et al. 2003; Frehlich and Sharman 2005; Zhang et al. 2003; Bradley et al. 2007). Among them, Sodar has a too short detection range, Lidar is not operational in foggy or rainy weathers and still very expensive to purchase and maintain, while Radar can detect and locate wake vortex within a relatively long distance under all weather conditions (Barbaresco and Meier 2010; Shariff and Wray 2002) and therefore appears as a promising choice. In recent years, a lot of experiments have been conducted to detect and monitor wake vortex. In Nespor et al. (1994), the vortices of a small fighter aircraft were detected at a range of 2.7km by using a 1MW C band pulse Doppler radar. In Shephard et al. (1994), GEC-Marconi research center executed wake vortex detection trials by using multi-functional coherent pulse Doppler radar in both S and X band. In Hanson and Marcotte (1997) and Iannuzzelli and Schemm (1998), the wake of C-130 aircraft was detected by an X band bi-static radar. In Barbaresco et al. (2007) and Barbaresco et al. (2008), the aircraft wake vortices at a range of 7 km was effectively detected by an X band

Radar in scanning mode, and the Radar Doppler signatures were observed in rainy weather as well as in clear air. In Seliga and Mead (2009), a W-Band Radar was used to detect wake vortices in rainy conditions and the reflectivity RHI plots showed clear evidence of enhanced droplet concentration between the vortices and reduced droplet concentration in columns directly below and towards the outside of each vortex. In Jameson and Kostinski (2010), the aircraft wake vortex was found to affect the backscattering properties of raindrops, because the perturbations of wake vortices may generate new periodic clustering in rain capable of increasing radar coherent backscatter.

Up to now, a significant part of the research on wake vortex radar sensors has been concentrated on field tests. On the other hand, theoretical studies on radar scattering mechanism of wake vortices also have been conducted to provide technological guidance for the development of new wake vortex radar sensors since 1990s. In clear air, the radar reflectivity of wake vortex is mainly caused by Bragg scattering from the refractive index fluctuations and some fruitful results have been achieved in Shariff and Wray (2002) and Li et al. (2011). In rainy weather, the Radar electromagnetic waves are not severely attenuated by raindrops or fog at short range. Contrarily, the droplets rolled up by the wake vortices are strong scatterers enhancing the intensity of the scattered signals. However, few studies on the radar backscattering of wake vortices in rainy weather have been reported. Thus, the main objective of the present work is to model and evaluate the radar signature of raindrops within wake vortices. Actually, the falling raindrops are transported by the wake turbulence flow as inertial particles under the influence of gravity and drag forces, their trajectories and velocities will be modified. Therefore the distribution of raindrops within wake vortices may be different from the one in still air, the spatial distribution and falling velocity of raindrops will be disturbed due to the drag induced by the air flow in the wake vortices. This disturbance will change the repartition and the speed of the droplets and may be sufficient to change the radar signature. This paper is organized as follows, the motion equation of raindrops in wake vortices is analyzed in section 2 and a simplified model to

compute the trajectory and velocity of raindrops within wake vortices is described in detail. In section 3, the computation of radar time series from raindrops in wake vortices based on the simulated drops sizes, positions and velocities is presented and the corresponding signal processing methods are described. In section 4, typical X band and W band radar signatures from raindrops within wake vortices are obtained and analyzed.

2. Motion of raindrops within wake vortices

Starting from the well known characteristics of the raindrops in terms of size distribution and terminal falling velocity in absence of turbulence, and considering a generic flow model for the vortex, a model to analyze the concentration of raindrops in the vicinity of the vortex is presented in this section. It will be used in a later stage to compute the radar signature of the raindrops within wake vortices.

a. Parametrization of raindrops in still air

Drop size distributions (DSD) have been widely used by radar-meteorologists as they can directly be related to the radar reflectivity (Marshall and Palmer 1948). Assuming spherical drops, the volumic distribution of their diameters D is usually described by a modified gamma distribution. For raindrops in a unit volume, the probability density function of the diameters $N(D)$ is given by

$$N(D) = N_0 D^{\mu} e^{-\wedge D}, m^{-4} \tag{1}$$

where $N_0(m^{-3}mm^{-1-\mu})$ is a constant reflecting the average spatial density of the drops and equal to 8×10^6 at the ground level, μ depends on the type of rain, and $\wedge$ is related to the rain rate R (in mm/h) by

$$\wedge = 4.1R^{-0.21}, mm^{-1} \tag{2}$$

Figure 1(a) presents the raindrops' size distributions for three different rain rates. In still air, a falling raindrop reaches its terminal fall velocity V_{T} with the equilibrium between the inertial force and the dragging force acting on it (Sauvageot 1992). A widely used exponential expression between V_{T} and the diameter D is given by (Fang 2003)

$$V_T(D) = [\alpha_1 - \alpha_2 exp(-\alpha_3 D)](\frac{\rho_0}{\rho})^{0.4}, m/s \tag{3}$$

where $\alpha_1 = 9.65m/s, \alpha_2 = 10.3m/s, \alpha_3 = 0.6m/s$. $(\rho_0/\rho)^{0.4}$ is a density ratio correction factor adjusting deviation of the terminal fall velocity due to the air density change with the fall level. Figure 1(b) presents the terminal fall velocity of raindrops for different altitude levels.

b. Wake vortex velocity profiles

In the atmosphere, the flow induced by the aircraft wake vortex introduces fluctuations of temperature, pressure, humidity and velocity field inside and outside the vortex core. The main effect of the vortex on a raindrop falling in the flow is a change of the drag force that is undergone by the drop due to the change of the relative velocity between the air flow and the drop. As shown in Figure 2, the aircraft vortex wake may be described by four specified zones and the vortex velocity profile in each zone is changing with time and space (Ginevsky and Zhelannikov 2009). In the wake formation zone, small vortices emerge from the vortex sheet at the wing tips and at the edges of the landing flaps. After rolled up, the wake enters into the stable phase, holding a relatively stable velocity profiles which may last for several minutes. In the following analysis, we focus on the fully rolled-up wake vortex in the stable phase.

In stable phase, the aircraft wake vortex is represented by superposing two coherently counter-rotating vortices with equal intensity and axis-symmetric velocity distributions, as shown in Figure 3. According to the Biot-Savart Law, the local flow velocity at the point P

can be expressed as

$$\mathbf{u}(x, y) = V_{\mathrm{L}} + V_{\mathrm{R}} + V_{\mathrm{d}} \tag{4}$$

where $V_{\mathrm{L}}, V_{\mathrm{R}}$ are the velocity components induced by the left and right vortex separately, V_{d} is the downwash velocity caused by the mutual interference between two vortices. In the following analysis of interaction between wake vortices and raindrops, V_{d} is neglected for the preliminary research.

For each single vortex, the widely-used Hallock-Burnham model is considered to depict its tangential velocity distribution. The tangential velocity fields from this model is expressed as (Gerz et al. 2002):

$$V_{\theta}(r) = \frac{\Gamma_0}{2\pi r} \cdot \frac{r^2}{r^2 + r_{\mathrm{c}}^2} \tag{5}$$

where $V_{\theta}(r)$ (m/s) is the tangential velocity at the distance r (m) from the vortex core, r_{c} (m) is the vortex core radius and $\Gamma_0(m^2/s)$ is the initial circulation determined mainly by the aircraft lift. In case of an elliptical distribution distribution of the lift, the circulation is expressed as

$$\Gamma_0 = \frac{Mg}{\rho U b_0}, b_0 = \frac{\pi}{4} b \tag{6}$$

where M(kg) is the weight of the airplane, U(m/s) is the flying speed, $g(m/s^2)$ is the gravitational acceleration, ρ is the air density, b_0 is the separation between two vortices, and $b(m)$ is the the aircraft's wingspan.

Figure 4 illustrates the two dimensional velocity distribution of the wake vortices generated by A340, whose maximum landing weight, landing velocity and wingspan are 259000 kg, 290 km/h, and 60.30 m respectively, each white arrow represents the velocity of the local vortex flow.

c. Motion equation of raindrops within wake vortices

To compute the trajectory of the raindrops in the neighborhood of the wake vortex some basic assumptions are made. Firstly, it is assumed that the raindrops are spherical and not

deformable. Secondly, the interaction between raindrops such as collision or coalescence, as well as the effects of wind and atmospheric turbulence on the raindrops, are not considered. Thirdly, the effects of the raindrops on the wake vortex flow are considered to be very small and negligible. Fourthly, no significant evaporation or condensation of the raindrops occurs in the vortex flow. Hence, the problem is simplified as a point particle dynamic problem.

As shown in Figure 5, the axis of the wake vortex is assumed to be perpendicular to the wake vortex flow between l and $l^{'}$. When a raindrop enters into the wake vortex flow at P, its movement is governed by

$$\mathbf{a}(t) = \frac{\mathbf{F}_{\mathrm{d}}(t)}{m_{\mathrm{p}}} + \mathbf{g} \tag{7}$$

where t is the time, $\mathbf{a}$ is the acceleration of the raindrop, $\mathbf{F}_{\mathrm{d}}$ is the fluid drag force acting on the raindrop, m_{p} is the mass of the raindrop, $\mathbf{g}$ is the downward gravitational acceleration which is taken as negative. For a raindrop moving with velocity $\mathbf{v}_{\mathrm{p}}$ in the fluid velocity field $\mathbf{u}[\mathbf{z}_{\mathrm{p}}(t)]$, if its diameter D is ranging from 0.5mm to 4mm, the Reynolds number of the flow is sufficiently high (Lovejoy and Schertzer 2008) to consider that the drag force $\mathbf{F}_{\mathrm{d}}$ is given by:

$$\mathbf{F}_{\mathrm{d}}(t) = \frac{1}{2} C_{\mathrm{d}} \rho_a \delta\mathbf{v}^2 \left(\frac{\pi D}{2}\right)^2, \delta\mathbf{v} = \mathbf{u}[\mathbf{z}_{\mathrm{p}}(t)] - \mathbf{v}_{\mathrm{p}}(t) \tag{8}$$

where $\mathbf{z}_{\mathrm{p}}(t)$ denotes the raindrop's position, $\delta\mathbf{v}$ is the relative velocity between the vortex flow and the raindrop, and C_{d} is the fluid drag coefficient. For a raindrop with diameter D and density ρ_{w}, the drag coefficient C_{d} is assumed to be constant as the impact of air density variations in the vortex flow on C_{d} is not taken into consideration. Thus, C_{d} can be derived by the equilibrium of its weight and the drag force in still air as:

$$C_{\mathrm{d}} = \frac{4\rho_w g D}{3\rho_a V_{\mathrm{T}}^2} \tag{9}$$

Submitting the equation 8 and 9 into equation 7, the motion equation of raindrops within

wake vortices can be further expressed as:

$$\begin{cases} \mathbf{a}(t) &= \mathbf{g} + \frac{g}{V_{\mathrm{T}}^2}|\delta\mathbf{v}|\delta\mathbf{v} \\ \frac{\mathrm{d}\mathbf{v}_{\mathrm{p}}(t)}{\mathrm{d}t} &= \mathbf{a}(t) \\ \frac{\mathrm{d}\mathbf{z}_{\mathrm{p}}(t)}{\mathrm{d}t} &= \mathbf{v}_{\mathrm{p}}(t) \end{cases} \tag{10}$$

The instantaneous position and velocity of raindrops can be obtained from the above equation. However, its nonlinearity does not enable its analytical computation. A procedure to solve this equation numerically is given in Appendix.

d. Trajectory of raindrops within wake vortices

For a raindrop falling from point P as shown in Figure 5, $PP^{'}$ and $PP^{"}$ demonstrate its trajectories within wake vortices and in still air respectively. In still air, the raindrop falls down along the trajectory which is vertical to the ground. In the presence of wake vortices, the trajectory of a raindrop is depending on the diameters of the raindrop and the location where it enters into the wake vortex flow. In Figure 6, the trajectories of four groups of raindrops with different diameters, namely: 0.5mm, 1mm, 2mm, 4mm are illustrated. The vertical position of the vortices is 150 meters above the ground. Initially, the raindrops are uniformly distributed on a horizontal plane 315.7 meters above the ground. The background color indicates the velocity of the two dimensional wake vortex flow. The white arrow denotes both the position and velocity of the raindrops at each time step. The trajectories of raindrops with smaller diameters seem to be more largely changed by vortex flow. The fall duration is defined as the total time the fastest moving raindrop takes from the initial position to the ground. The fall duration of the 0.5mm group of raindrops is longer than the fall duration of other groups of raindrops, as their terminal falling velocity is much lower than the ones of larger drops. In some part of the region under the vortex flow, there are no raindrops falling down. In the region between the two vortex cores, some of raindrops are preferentially concentrated due to the influence of the vortex velocity field, the velocities of the raindrops here are also considerably increased.

3. Radar signature of raindrops in wake vortices

The signal arriving from the scattering volume that contains raindrops can be used to retrieve parametrical information on the raindrop through the interpretation of the Doppler information as already widely used for weather monitoring purposes. In the present case, the heterogenous distribution and velocities of the raindrops perturbed by the vortex flow should induce a distinct signature from the one obtained from volumes with raindrops in still air. The radar signature of the raindrops in the vicinity of wake vortices is modeled and analyzed in the following of this section.

a. Microwave properties of raindrops

Considering a spherical raindrop of diameter D (m) and an incident electromagnetic wave of wavelength λ (m), the radar backscattering cross section of the raindrop is closely related to its radio-electric size $\alpha = \pi D/\lambda$. α is generally smaller than 1 for a wide range of radar bands (S, C, X bands), because the sizes of raindrop scatterers are smaller than the wavelengths. In this case, the radar cross section of a raindrop is well described by the Rayleigh approximation (Gunn and East 1954)

$$\sigma = \frac{\pi^5}{\lambda^4}|K|^2 D^6, K = \frac{m^2-1}{m^2+2} \tag{11}$$

where $|K|^2$ is a coefficient related to the dielectric constant of water, m is the complex refractive index of the raindrops relative to the air background and can be expressed as $m = n - ik$. $n = \sqrt{\varepsilon_r}$ is the ordinary refractive index with ε_r the constant dielectric, and k the absorption coefficient of the raindrops. In Rayleigh approximation region, temperature change doesn't affect the scattering greatly. Practically, $|K|^2$ could be considered as constant for radar application at temperatures found in the atmosphere and centimetric wavelengths (Sauvageot 1992). In the following simulation, $|K|^2 = 0.93$ is adopted. For higher frequency bands, if α is comparable to 1, the backscattering cross section of a raindrop is usually given

by Mie formulas

$$\sigma = \frac{\lambda^2}{4\pi}\left|\sum_{n=1}^{\infty}(-1)^n(2n+1)(a_n - b_n)\right|^2 \tag{12}$$

where a_n and b_n are the "Mie Coefficients" obtained from Bessel and Hankel functions with arguments α and m. Detailed expressions for computation can be found in (Sauvageot 1992). In Figure 7, the backscattering cross section function of raindrop's diameter, is computed by Rayleigh and Mie formulas for 10 GHz and 94 GHz incident waves respectively.

b. Radar Signal time series

Combining the results of the previous section, it is at this stage possible to simulate the radar echo from the raindrops in wake vortex region in any configuration. As shown in Figure 8, a radar pointing perpendicularly to the rotation axis of wake vortex, with an elevation angle α_0 is firstly considered. The distance between the Radar and the airport runway is $R_{\mathbf{0}}$, the height of the wake vortex core is h_0. Above the wake vortex region, the raindrops are assumed to be homogeneously distributed as shown in Equation 1. In the area impacted by the vortex flow in stable stage, the new size distribution of raindrops is obtained by numerical computation of the motion equation 10 and is assumed to be stationary once the smallest raindrops just above the vortices reach the ground. In the following analysis, we consider the radar echo model of raindrops in a given resolution volume which is defined by the radar range resolution and the beam widths of the radar antenna.

Supposing that the Doppler radar transmits a series of N_{p} pulses with unitary normalized amplitudes

$$s_0(t) = \exp(j2\pi f_{\mathrm{c}} t)\sum_{n=0}^{N_{\mathrm{p}}-1}\mathrm{rect}\left(\frac{t-nT}{\tau}\right)\mu(t-nT) \tag{13}$$

where f_{c} is the carrier frequency of the signal, T is the pulse repetition interval, and τ is the pulse width. rect$(*)$ is a rectangular function equal to 1 for $0 \leq * \leq 1$ and to 0 otherwise, $\mu(t)$ is a pulse modulation function which can be set as linear frequency modulation, or phase coded modulation. Here the simplest situation with $\mu(t) = 1$ is considered. Considering

the kth raindrop in the given resolution volume, at time t=0, it is positioned with the coordinates (r_k, α_k, ϕ_k) while the radar antenna beam is pointed to the direction of (α_0, ϕ_0), the backscattered baseband signal of this raindrop from the nth pulse can be expressed as follows

$$s_k(n) = A_k \exp\left[-j2\pi f_c \frac{2(r_k + nTv_k)}{c}\right] \tag{14}$$

where c is the speed of light, v_k is the radial velocity of the raindrop moving towards the radar, A_k is the amplitude of the signal which is derived from the radar equation with the following analytical form

$$A_k = H\frac{\sqrt{\sigma_k}}{r_k^2} w_{\mathrm{a}}(\alpha_k, \phi_k) w_{\mathrm{r}}(r_k), H = \sqrt{\frac{P_{\mathrm{t}} G^2 \lambda^2}{(4\pi)^3 L}} \tag{15}$$

where P_{t} is the transmitted power, G is the antenna gain, λ is the wavelength, L is the total loss of the radar system, σ_k is the radar cross section of the raindrop, and w_{a} and w_{r} are the angular and radial weighting functions respectively, depending on the location of the raindrop in the radar scattering volume (Cheong et al. 2008; Capsoni and DAmico 1998; Capsoni et al. 2001). Thus, the composite signal time series reflected from the transmitted pulses can be approximated by the superimposition of the baseband signals backscattered from all the raindrops in the radar scattering volume

$$S_r(n) \quad = \quad \sum_{k=1}^{N_{\mathrm{r}}} s_k(n) + n_s \tag{16}$$

where N_{r} represents the number of raindrops in the given resolution volume, n_s is a centered complex Gaussian white noise. In our analysis, the multiple scattering of raindrops is ignored and the ground clutter competing with the raindrops' signatures is not taken into account as it can be easily removed (Richards et al. 2010).

Based on the above equation, the radar echo of a given resolution volume can be computed for each transmitted pulse. It is worthy pointing out that the coordinates of each raindrop is changing for different pulses due to their motion in wake vortex flow, the mathematical relationship between its coordinates and its position in two dimensional wake vortex region

can be obtained through the computation of the motion equation. At each instant when the radar transmits a pulse, the positions and velocities of the raindrops are updated according to the motion equation by numerical simulation. A general description of the procedure to compute the radar signal time series of raindrops in wake vortices is summarized in Figure 9.

c. Radar Signal Processing

The radar reflectivity and Doppler spectrum characteristics are of great importance in the radar observation of meteorological targets. In radar meteorology, the reflectivity of raindrops is defined as the sum of the backscattering cross sections of the each individual raindrops over the unit volume:

$$\eta = \frac{1}{V}\sum_{V}\sigma_k \tag{17}$$

which implies that the raindrops are homogeneously distributed in the given radar resolution volume. However, the spatial distribution of raindrops moving in the wake vortex flow is no longer homogeneous. Therefore, we introduce the equivalent radar cross section σ_v, to represent the radar reflectivity of raindrops in the given resolution volume. One of the advantages to calculate σ_v is that, for the radar observation of wake vortex in rainy weather conditions, the RCS contribution of the raindrops due to the Rayleigh scattering could then be compared with the RCS of the wake vortex due to the Bragg scattering induced by the refractivity gradient within the flow as studied in (Myers and Scales 1999; Shariff and Wray 2002; Li et al. 2009, 2011). Assuming that the angular and radial weighting functions be equivalent to 1, σ_v can be approximately derived from the Radar equations as

$$\sigma_v = \frac{r_0^4}{H^2}P_r \tag{18}$$

where r_0 denotes the distance from the radar to the center of the radar resolution volume, H is the constant defined in Eq. (15), P_r is the average received power which can be obtained easily by analyzing the Doppler spectrum of the recorded or simulated radar time series

$S_r(n)$ and summing the power spectrum over all the Doppler spectrum bins as

$$P_r = \sum_{m=1}^{N_\mathrm{p}} Y(m)\Delta f_\mathrm{d} \tag{19}$$

where N_p is the number of coherent integration pulses, Δf_d is the Doppler frequency resolution, $Y(m)$ denotes the energy contribution to the Doppler spectrum from each Doppler frequency bin. Under the condition of short radar time series, a number of high resolution spectral estimation methods, including the maximum entropy method and parametric methods, can be utilized to estimate the Doppler spectrum of the $S_r(n)$ as well (Barbaresco and Meier 2010). Actually, the Doppler velocity is proportional to the Doppler frequency via the relationship $v_\mathrm{d} = 2\lambda f_\mathrm{d}$, thus, the Doppler spectrum is a power-weighted distribution of raindrops radial velocities within the radar resolution volume (Yu et al. 2007). In the wake vortex region, the raindrops move towards various directions which are determined by the combination of drag forces and gravity, the Doppler spectrum will be broadened correspondingly. The width of the Doppler spectrum is very significant to identify the possible wake vortex warnings, the estimation of its location and strength, as well as the prediction of wake vortex evolutions.

4. Simulation and Discussion

In this section, typical X band radar and W band radar are assumed to be used for monitoring aircraft wake vortices in rainy weather. From the model of interactions between raindrops and wake vortices, considering a given radar configuration, the radar signatures of raindrops within wake vortices are here illustrated by numerical simulation. The main objectives of the simulation are to estimate the Doppler velocity spectrum of raindrops within wake vortex and to evaluate the radar detectability of wake vortex in rainy weather. The simulation results are expected to develop knowledge on wake vortex radar sensors.

a. Initial position of raindrops

The first step in the simulation is to generate the initial distribution of raindrops in the wake vortex region. As shown in Figure 8, in the region above the wake vortex, the raindrops size distribution is assumed to be homogeneous. At each time step, some of the raindrops will enter into the wake vortex region, their positions and velocities are updated from the numerical computation of the motion equation. The procedure is continued until the smallest raindrops reach the ground or pass through the wake vortex region. Figure 10 illustrates the simulated position of the drops in the wake vortices at the initial time of the radar simulations, the raindrops with diameters of 0.5mm, 1mm, 2mm, 3mm and 4mm are displayed in a two-dimensional plane. The rain rate is assumed to be 5 mm/h and the wake vortex characteristics correspond to the characteristics of a stable stage wake vortex generated by a A340. It is interesting to note the enhanced concentration of raindrops between the two vortices and the reduced concentration of raindrops in the columns below the two vortices. Indeed this heterogeneous concentration of raindrops is one of the element that may enable a detection of the vortices.

b. X band Radar Doppler signatures

X-band radar is an interesting sensor for monitoring wake vortex due to its high temporal and spatial resolution and the low cost. In the vicinity of the airport, the attenuation of X band radar in rainy weather is not serious due to the short detection range of wake vortices. In the simulation, the rain rate is set to be 5mm/h and the input radar parameters are listed in Table 1, referring to the X band radar parameters for monitoring wake vortices described in Barbaresco and Meier (2010). In order to exploit more about the Doppler signature of raindrops within wake vortices, different radar geometry configurations are considered as shown in Figure 11.

In Figure 11(a), the concerned radar scattering volume is divided into 6 continuous range

cells where the two vortex cores are located in two adjacent cells, and the range resolution is 40 meters. The elevation angle of the radar beam is 5°. Figure 12 shows the obtained Doppler spectrum of radar echo in the 6 considered radar cells. It can be noticed that the width of the Doppler spectrum is wider for radar cell 02-05, and especially for cell 03 and 04 with regards to cell 1 and 6 that are further from the vortex cores. Actually this phenomenon is caused by the richness of radial velocities of the scattered raindrops in the given radar cell, as well as the inhomogeneous concentration of raindrops in the wake vortex region. In Barbaresco and Meier (2010), the Doppler spectrum of wake vortex in clear air was also found to be extended, but with several symmetrical peak values due to its spiral geometry. This extended Doppler spectrum indication is a possible signature that denotes the existence of wake vortex.

In Figure 11(b), the two vortex cores are located in two interval radar cells and the radar echoes from five successive radar cells are simulated. In Figure 13, the Doppler velocity spectrum from the raindrops in the three radar cells around the vortices are illustrated. The elevation angle of the antenna is configurable to be 3°, 5° and 7° as shown in Figure 11(c). It is easily found that the width of Doppler velocity spectrum is depending on the elevation angle. At the elevation angle of 3°, the antenna beam is pointing to the raindrops below the wake vortex cores, the richness of radial velocities of raindrops is less than the one at 5° and 7° of elevation.

In Figure 11(d), two vortex cores are located in the same radar resolution volume while the range resolution is set to 100 m. The corresponding Doppler velocity spectrum is illustrated in Figure 14. In radar cell 01 and 03, the Doppler velocity spectrum of raindrops is not extended and almost the same as in still air. In radar cell 02, the Doppler velocity spectrum is almost symmetrically distributed and the width is also depending on the elevation angle. Actually, the raindrops size distribution in each pulse resolution volume is depending on the division of the radar cells which are defined by the pulse width and the radar antenna beam width.

c. W band Radar Doppler signatures

Other recent radar trials to detect wake vortex in rainy weather have been reported in Seliga and Mead (2009). The parameters of the W band radar used for the experiments are illustrated in Table 2. Considering the proposed methodology, this measurement configuration is taken as a reference to simulate the radar signature of the raindrops in wake vortices. The altitude of the A340 wake vortices is assumed to be 200m above the airport runway and the radar is deployed 1000m away from the runway. The W band radar is working in vertical scanning mode, with a scan rate of $5°/s$. The rain rate is set to be 2 mm/h. The received radar time series at the each radar cell are processed to obtain the average power and the Doppler velocity field. In Figure 15, the average received power and the corresponding Doppler velocity are illustrated separately. The simulated results are very similar to the W-Band Radar observation by T. A. Seliga in 2009. In the scanned radar reflectivity map, there are two columns with reduced reflectivity from raindrops due to the presence of a pair of wake vortices. Between these two columns, there are several radar cells with enhanced radar reflectivity due to the enhanced concentration of raindrops within wake vortices. The difference in the radar reflectivity level is about 6 dB (the absolute value is not comparable as the number of simulated raindrops is far lower than the actual one to get reasonable computing times). For the retrieved Doppler velocity map, both the negative and positive peak Doppler velocities are obtained in radar cells around the vortex cores asymmetrically. This kind of information on the radial velocity of raindrops within wake vortices is critical to estimate the vortex circulation for air traffic control application, as related to the danger associated with a wake vortex encountering. It has to be noticed that due to the low dimensions of the radar cells and the low number of simulated drops the simulated doppler information is not relevant in the radar cells with an extremely low reflectivity (i.e under the vortex cores).

5. Conclusion

This paper has presented a methodology to simulate the radar signature of wake vortices in rainy conditions. The theoretical model for the computation of raindrops' trajectories within wake vortices, as well as the interaction between raindrops and electromagnetic waves, have been presented. The radar echo is then computed considering all the raindrops within the observation volume. The enhanced concentration of raindrops between the two vortex cores due to the influence of vortex flow is clearly observed by numerical simulation. To some extent, this phenomenon is consistent with the experimental results by (Seliga and Mead 2009). The particular shape of the Doppler spectrum of the raindrops within wake vortices can provide potential information for identifying wake vortex hazard in air traffic control. The simulation results will lately be validated by the radar data of wake vortex observation in rainy weather. At this stage, the relevance of some of the simplifications and assumptions will be evaluated and if needed, the effect of wind and turbulence on the raindrops' motion or collision between raindrops will be taken into account. The simulated radar signature of wake vortices will then be used to evaluate different algorithms to detect vortices from the radar signal and also to retrieve some vortex parameters such as the circulation or the vortex core separation and radius. It will hence enable to assess the most relevant radar configurations for the observation of wake vortices in rainy weather.

Acknowledgments.

The authors would like to thank Mr. Florent Christophe (ONERA/DEMR) and Mr. Frederic Barbaresco (THALES AIR OPERATIONS) for their helpful supervisions of this work.

APPENDIX

Numerical solution to the motion equation

In Eq. (10), four variables concerning the motion of raindrops need to be determined, including the positions and velocities of the raindrops in a 2D plane orthogonal to the vorticity axis of the vortices: $x_{\rm p}, y_{\rm p}, v_x,$ and v_y. The Runge-Kutta algorithm is widely used for numerically solving non-linear differential equations, with high accuracy and good performance. A 4th order four variables Runge-Kutta algorithm has been developped to compute the above motion equation. The corresponding differential equations for these four variables can be written as:

$$\begin{cases} \frac{{\rm d}x_{\rm p}}{{\rm d}t} = f_1(x_{\rm p}, y_{\rm p}, v_x, v_y) = v_x \\ \frac{{\rm d}y_{\rm p}}{{\rm d}t} = f_2(x_{\rm p}, y_{\rm p}, v_x, v_y) = v_y \\ \frac{{\rm d}v_x}{{\rm d}t} = f_3(x_{\rm p}, y_{\rm p}, v_x, v_y) = \frac{g}{V_{\rm T}^2}|\delta\mathbf{v}|[u_x(x_{\rm p}, y_{\rm p}) - v_x] \\ \frac{{\rm d}v_y}{{\rm d}t} = f_4(x_{\rm p}, y_{\rm p}, v_x, v_y) = -g + \frac{g}{V_{\rm T}^2}|\delta\mathbf{v}|[u_y(x_{\rm p}, y_{\rm p}) - v_y] \end{cases} \tag{A1}$$

where the initial position of the raindrop is thought to be located far away from the vortex core and the initial velocity of the raindrop is set to be its terminal velocity in still air. In the above equations, there are no derivatives on the right hand side, and there are only first derivatives on the left hand side. Therefore, these equations can be summarized in vector form as

$$\mathbf{X}' = \mathbf{f}(\mathbf{X}) \tag{A2}$$

where $\mathbf{X} = (x_{\rm p}, y_{\rm p}, v_x, v_y)$ is the vector of the raindrop parameters and $\mathbf{f} = (f_1, f_2, f_3, f_4)$ is the vector of functions. Considering an adaptive time interval of length Δt, the raindrop vector $\mathbf{X}$ could be labeled as $\mathbf{X}_n$ and $\mathbf{X}_{n+1}$ at any two continuous time shots t_n and t_{n+1} where $t_{n+1} = t_n + \Delta t$. If the raindrops parameters at time t_n is supposed to be already

known as $\mathbf{X}_n = (x_{\mathrm{p,n}}, y_{\mathrm{p,n}}, v_{x,n}, v_{y,n})$ and in order to compute the raindrop parameters $\mathbf{X}_{n+1}$ at time t_{n+1} by the 4th order Runge-Kutta algorithm, the estimates of the derivative of $\mathbf{X}$ at the time interval from t_n to t_{n+1} can be described as the following procedures:

$$\begin{cases} \mathbf{a}_n = \mathbf{f}(\mathbf{X}_n) \\ \mathbf{b}_n = \mathbf{f}(\mathbf{X}_n + \frac{1}{2}\Delta t \mathbf{a}_n) \\ \mathbf{c}_n = \mathbf{f}(\mathbf{X}_n + \frac{1}{2}\Delta t \mathbf{b}_n) \\ \mathbf{d}_n = \mathbf{f}(\mathbf{X}_n + \Delta t \mathbf{c}_n) \end{cases} \tag{A3}$$

where $\mathbf{a}_n$ is the value at beginning of time interval, $\mathbf{b}_n$ and $\mathbf{c}_n$ are two estimates of values at the mid-point, and $\mathbf{d}_n$ is the estimate of value at end of time interval. Therefore, $\mathbf{X}_{n+1}$ can be finally computed as the weighted sum of the above estimates of derivatives:

$$\mathbf{X}_{n+1} = \mathbf{X}_n + \frac{1}{6}(\mathbf{a}_n + 2\mathbf{b}_n + 2\mathbf{c}_n + \mathbf{d}_n)\Delta t \tag{A4}$$

where $\mathbf{X}_0$ is equal to $\mathbf{X} = (x_0, y_0, 0, V_{\mathrm{T}})$.

REFERENCES

Barbaresco, F., A. Jeantet, and U. Meier, 2007: Wake vortex detection & monitoring by x-band doppler radar : Paris orly radar campaign results. *Proc. IET Int Radar Systems Conf*, 1–5.

Barbaresco, F. and U. Meier, 2010: Radar monitoring of a wake vortex: Electromagnetic reflection of wake turbulence in clear air. *C. R. Physique*, **11**, 54–67.

Barbaresco, F., J. P. Wasselin, A. Jeantet, and U. Meier, 2008: Wake vortex profiling by doppler x-band radar : Orly trials at initial take-off & ils interception critical areas. *Proc. IEEE Radar Conf. RADAR '08*, 1–6, doi:10.1109/RADAR.2008.4721113.

Bobylev, A. V., V. V. Vyshinsky, G. G. Soudakov, and V. A. Yaroshevsky, 2010: Aircraft vortex wake and flight safety problems. *Journal of Aircraft*, **47**, 663–674.

Bradley, S., E. Mursch-Radlgruber, and S. von H?nerbein, 2007: Sodar measurements of wing vortex strength and position. *J. Atmos. Oceanic Technol.*, **24 (2)**, 141–155, URL `http://dx.doi.org/10.1175/JTECH1966.1`.

Capsoni, C. and M. DAmico, 1998: A physically based radar simulator. *J. Atmos. Oceanic Technol.*, **15**, 593–598.

Capsoni, C., M. D'Amico, and R. Nebuloni, 2001: A multiparameter polarimetric radar simulator. *J. Atmos. Oceanic Technol.*, **18**, 1799–1809.

Cheong, B. L., R. D. Palmer, and M. Xue, 2008: A time series weather radar simulator based on high-resolution atmospheric models. *J. Atmos. Oceanic Technol.*, **25 (2)**, 230–243, doi: 10.1175/2007JTECHA923.1, URL `http://journals.ametsoc.org/doi/abs/10.1175/`

2007JTECHA923.1, http://journals.ametsoc.org/doi/pdf/10.1175/2007JTECHA923.1.

Fang, F., 2003: Raindrop size distribution retrieval and evaluation using an s-band radar profiler. M.S. thesis, B.S.E.E. University of Central Florida, 180 pp.

Frehlich, R. and R. Sharman, 2005: Maximum likelihood estimates of vortex parameters from simulated coherent doppler lidar data. *J. Atmos. Oceanic Technol.*, **22 (2)**, 117–130, URL http://dx.doi.org/10.1175/JTECH-1695.1.

Gerz, T., F. Holzpfel, and D. Darracq, 2002: Commercial aircraft wake vortices. *Progress in Aerospace Sciences*, **38 (3)**, 181 – 208, doi:DOI:10.1016/S0376-0421(02)00004-0, URL http://www.sciencedirect.com/science/article/B6V3V-45NGHXY-1/2/55b701827ff6de230fe11e9c08c7b196.

Ginevsky, A. and A. Zhelannikov, 2009: *Vortex Wakes of Aircrafts, Foundations of Engineering Mechanics,*. Springer-Verlag Berlin Heidelberg, doi:10.1007/978-3-642-01760-5_1.

Gunn, R. L. S. and T. W. R. East, 1954: The microwave properties of precipitation particles. *Quarterly Journal of the Royal Meteorological Society*, **80**, 522–545.

Hanson, J. M. and F. J. Marcotte, 1997: Aircraft wake vortex detection using continuous-wave radar. *Johns Hopkins APL Technical Digest*, **18**, 348–357.

Holzpfel, F., T. Gerz, F. Kpp, E. Stumpf, M. Harris, R. I. Young, and A. Dolfi-Bouteyre, 2003: Strategies for circulation evaluation of aircraft wake vortices measured by lidar. *J. Atmos. Oceanic Technol.*, **20 (8)**, 1183–1195, URL http://dx.doi.org/10.1175/1520-0426(2003)020<1183:SFCEOA>2.0.CO;2.

Iannuzzelli, R. J. and C. E. Schemm, 1998: Aircraft wake detection using bistatic radar: Analysis of experimental results. *Johns Hopkins APL Technical Digest*, **19**, 299–314.

Jameson, A. R. and A. B. Kostinski, 2010: Partially coherent backscatter in radar observations of precipitation. *J. Atmos. Sci.*, **67 (6)**, 1928–1946, doi:10.1175/2010JAS3336.1, URL `http://journals.ametsoc.org/doi/abs/10.1175/2010JAS3336.1`, `http://journals.ametsoc.org/doi/pdf/10.1175/2010JAS3336.1`.

Li, J., X. Wang, and T. Wang, 2011: Modeling the dielectric constant distribution of wake vortices. **47 (2)**, 820 –831, doi:10.1109/TAES.2011.5751228.

Li, J., X. Wang, T. Wang, and Z. Liu, 2009: Study on the scattering characteristics of stable-stage wake vortices. *IEEE International Radar Conference*, Paris.

Lovejoy, S. and D. Schertzer, 2008: Turbulence, raindrops and the l1/2 number density law. *New J. Phys.*, **10**, 075 017 (32pp), doi:10.1088/1367-2630/10/7/075017.

Marshall, J. S. and W. M. Palmer, 1948: The distribution of raindrops with size. *J. Meteorol.*, **5**, 165–166.

Myers, T. J. and W. A. Scales, 1999: Determination of aircraft wake vortex radar cross section due to coherent bragg scatter from mixed atmospheric water vapor. *Radio Science*, **34 (1)**, 103C111.

Nespor, J. D., B. Hudson, R. L. Stegall, and J. E. Freedman, 1994: Doppler radar detection of vortex hazard indicators. Tech. rep., NASA. Langley Research Center.

Proctor, F. H., D. W. Hamilton, D. K. Rutishauser, and G. F. Switzer, 2004: Meteorology and wake vortex influence on american airlines fl-587 accident. Tech. Rep. 213018, Langley Research Center, NASA.

Richards, M. A., j. A. Scheer, and W. A. Holm, 2010: *Principles of modern radar: Basic principles*. SciTech Publishing, Inc.

Rubin, W. L., 2000: Radar-acoustic detection of aircraft wake vortices. *J. Atmos. Oceanic Technol.*, **17 (8)**, 1058–1065, URL http://dx.doi.org/10.1175/1520-0426(2000)017<1058:RADOAW>2.0.CO;2.

Sauvageot, H., 1992: *Radar Meteorology*. Artech House, 366 pp.

Seliga, T. A. and J. B. Mead, 2009: Meter-scale observations of aircraft wake vortices in precipitation using a high resolution solid-state w-band radar. *The 34th conference on Radar Meteorology*.

Shariff, K. and A. Wray, 2002: Analysis of the radar reflectivity of aircraft vortex wakes. *J. Fluid Mech*, **463**, 121C161.

Shephard, D., A. Kyte, and C. Segura, 1994: Radar wake vortex measurements at f and i band. 7/1 –7/5.

Yu, T.-Y., Y. Wang, A. Shapiro, M. B. Yeary, D. S. Zrni?, and R. J. Doviak, 2007: Characterization of tornado spectral signatures using higher-order spectra. *J. Atmos. Oceanic Technol.*, **24 (12)**, 1997–2013, URL http://journals.ametsoc.org/doi/abs/10.1175/2007JTECHA934.1.

Zhang, Y., F. Y. Wang, and J. C. Hardin, 2003: Spectral characteristics of wake vortex sound during roll-up. Tech. rep., NASA.

List of Tables

TABLE 1. Input parameters of the X band radar simulation

Parameters	Values
Radar frequency	10GHz
Transmitted peak power	20W
Noise figure	2dB
System Loss	3dB
Antenna gain	30dB
Beam width	$2.8^\circ \times 4^\circ$
Distance of wake vortex	500 m
Pules Repetition Frequency	3348Hz
Number of pulses	256

TABLE 2. Input parameters of the W band radar simulation

Parameters	Values
Radar frequency	94GHz
Transmitted peak power	100 mW
Noise figure	12dB
Antenna gain	58dB
Beam width	0.18°
Azimuth angle	0°
Elevation angle	7° - 14°
Antenna scanning rate	$5°/s$
Range resolution	2m
Pules Repetition Frequency	20 kHz

List of Figures

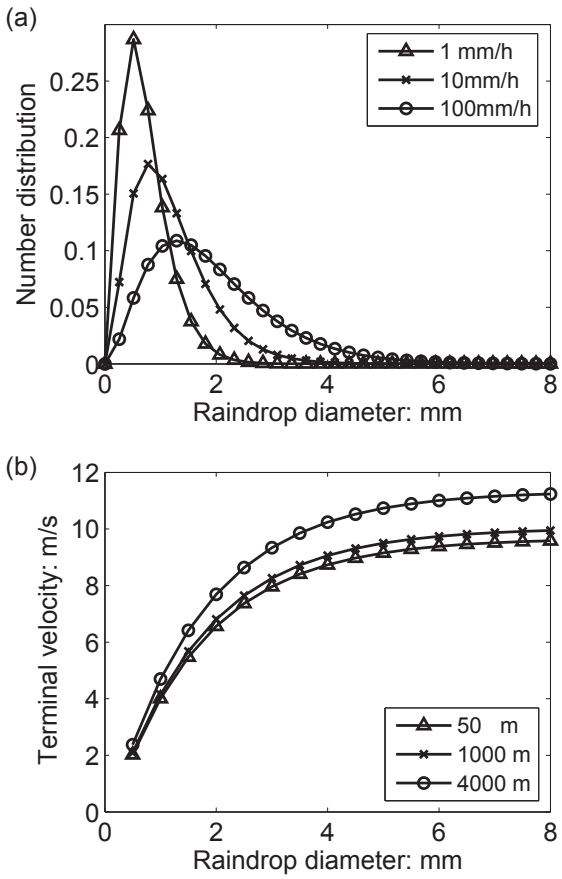

FIG. 1. Some characteristics of raindrops in still air: (a) Raindrops size distribution and (b) Terminal falling velocity

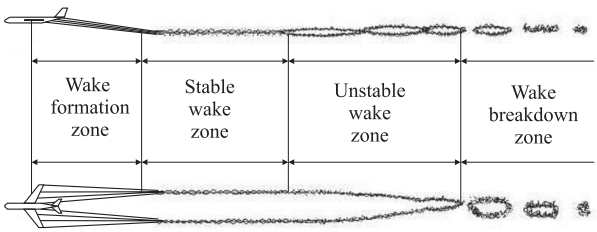

FIG. 2. Breakdown of the aircraft vortex wake in accordance with its evolution phases (Ginevsky and Zhelannikov 2009)

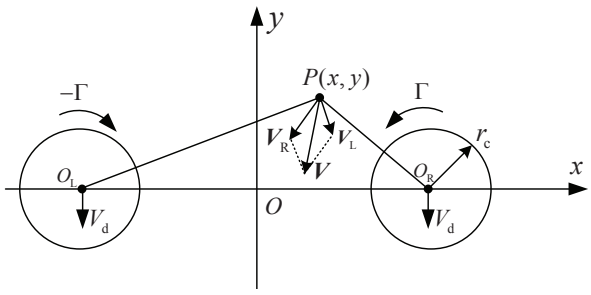

FIG. 3. The velocity field of two counter-rotating vortices (Li et al. 2011)

.

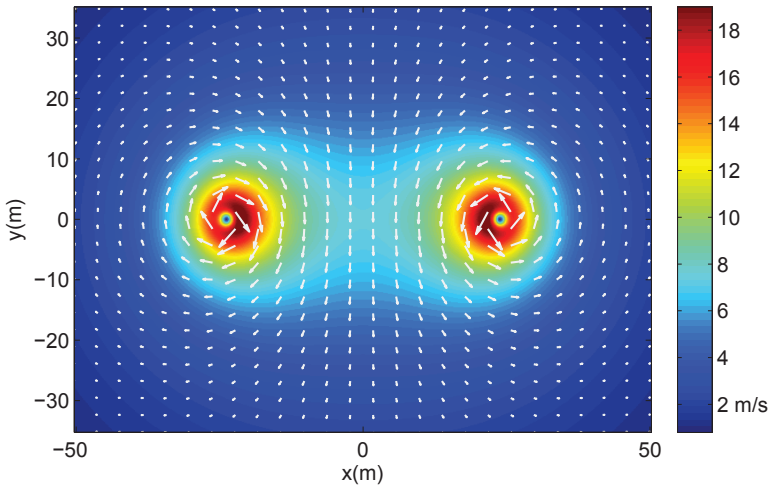

FIG. 4. Two dimensional velocity distribution of the wake vortices generated by A340

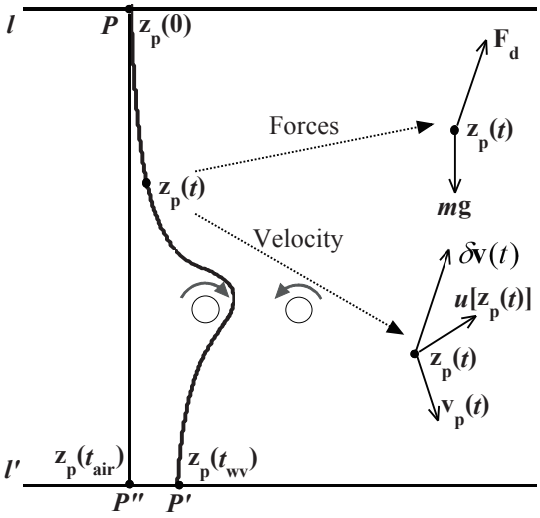

FIG. 5. Interaction between Raindrops and Wake Vortices

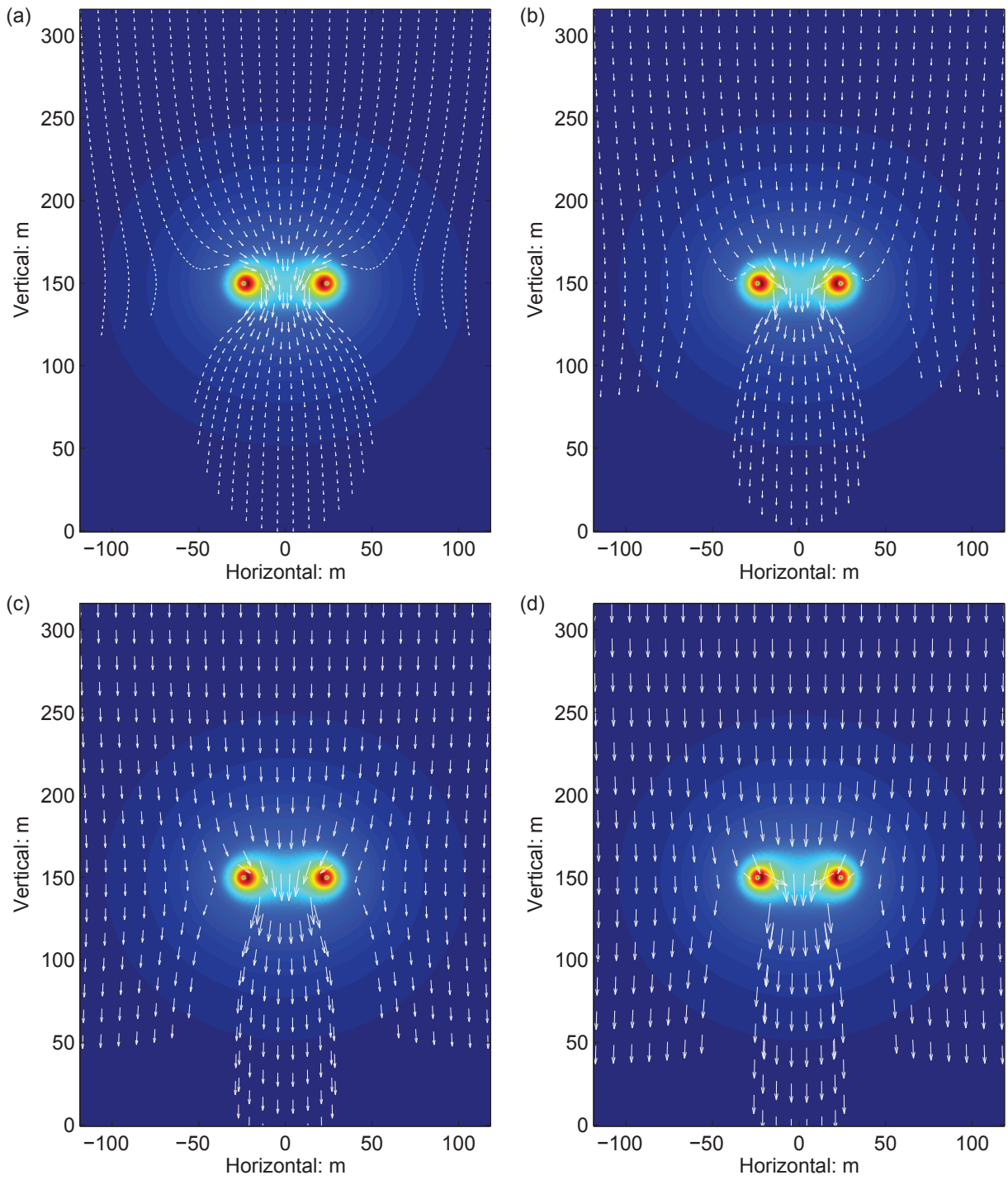

FIG. 6. The trajectory of raindrops in wake vortices: (a)D=0.5mm, Duration:106.6s, (b)D=1.0mm, Duration:62.2s, (c)D=2.0mm, Duration:41.0s, (d)D=4.0mm, Duration:31.8s

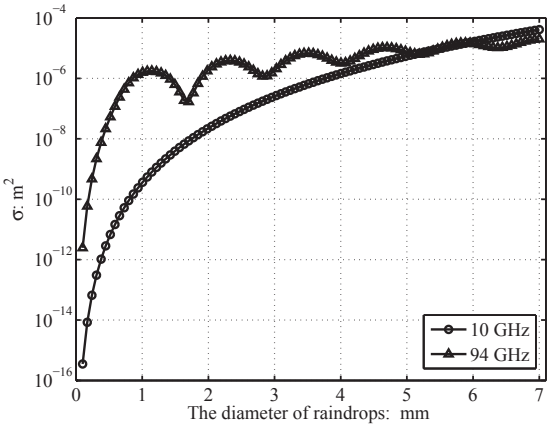

FIG. 7. Backscattering cross section of a raindrop in function of its diameter

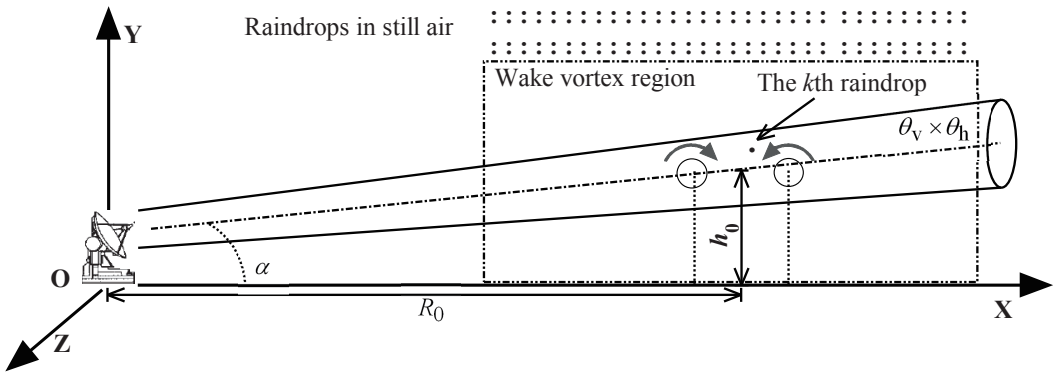

FIG. 8. The geometry of radar configuration

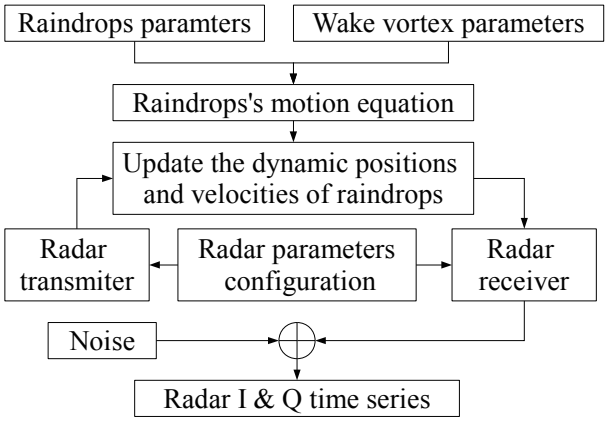

FIG. 9. The procedure of generating radar signal time series

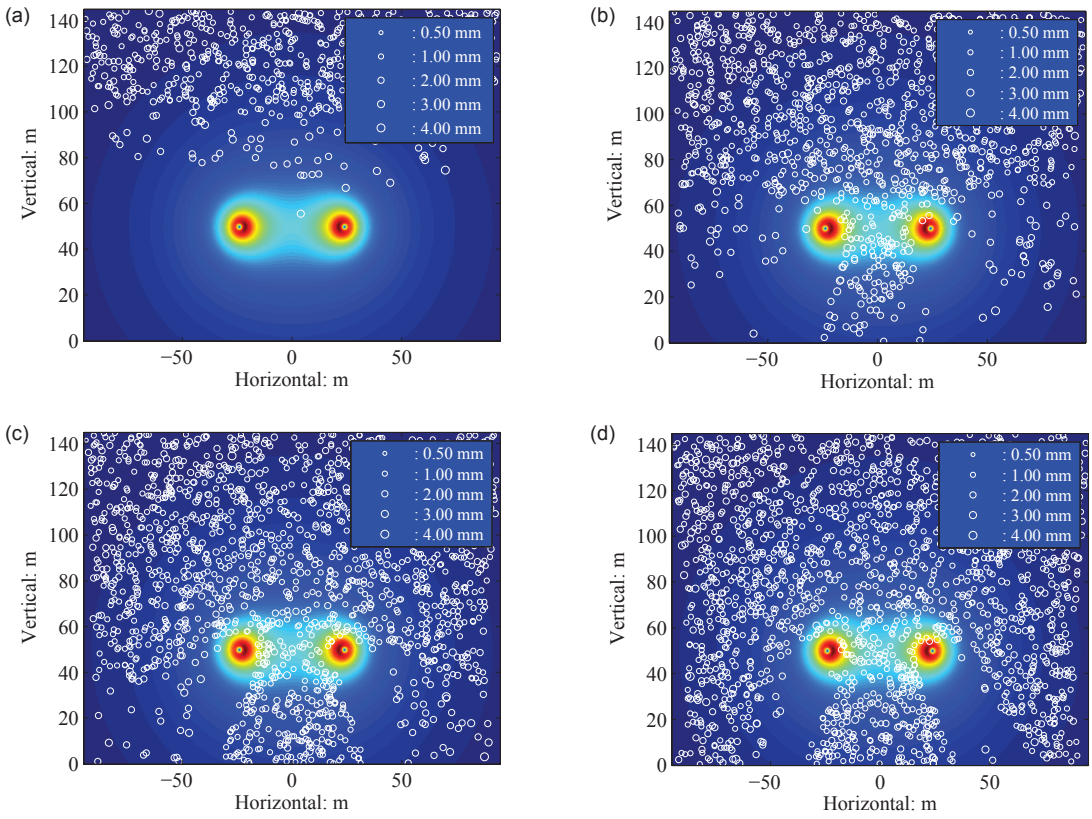

FIG. 10. Generation of raindrops within wake vortices before computation of the radar signal: (a)Time:12.5s, (b)Time:25s, (c)Time:37.5s, (d)Time:50s

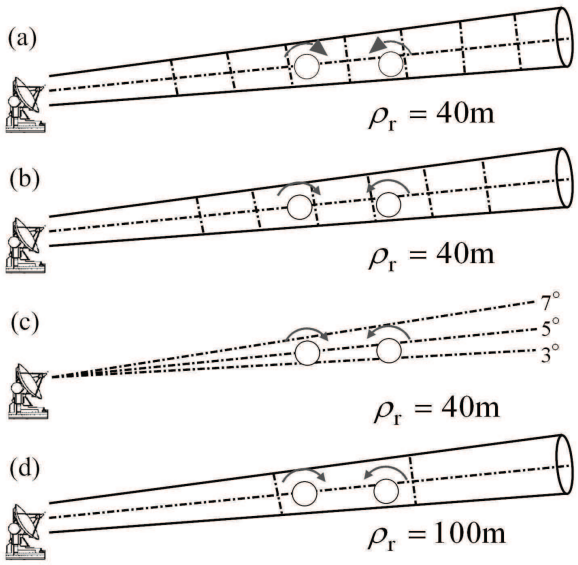

FIG. 11. Different radar geometry configurations for X band simulation: (a)Two vortex cores in two adjacent cells, (b)Two vortex cores in two interval cells, (c)Elevation angles: 3°, 5°, 7°, (d)Range resolution: 100m

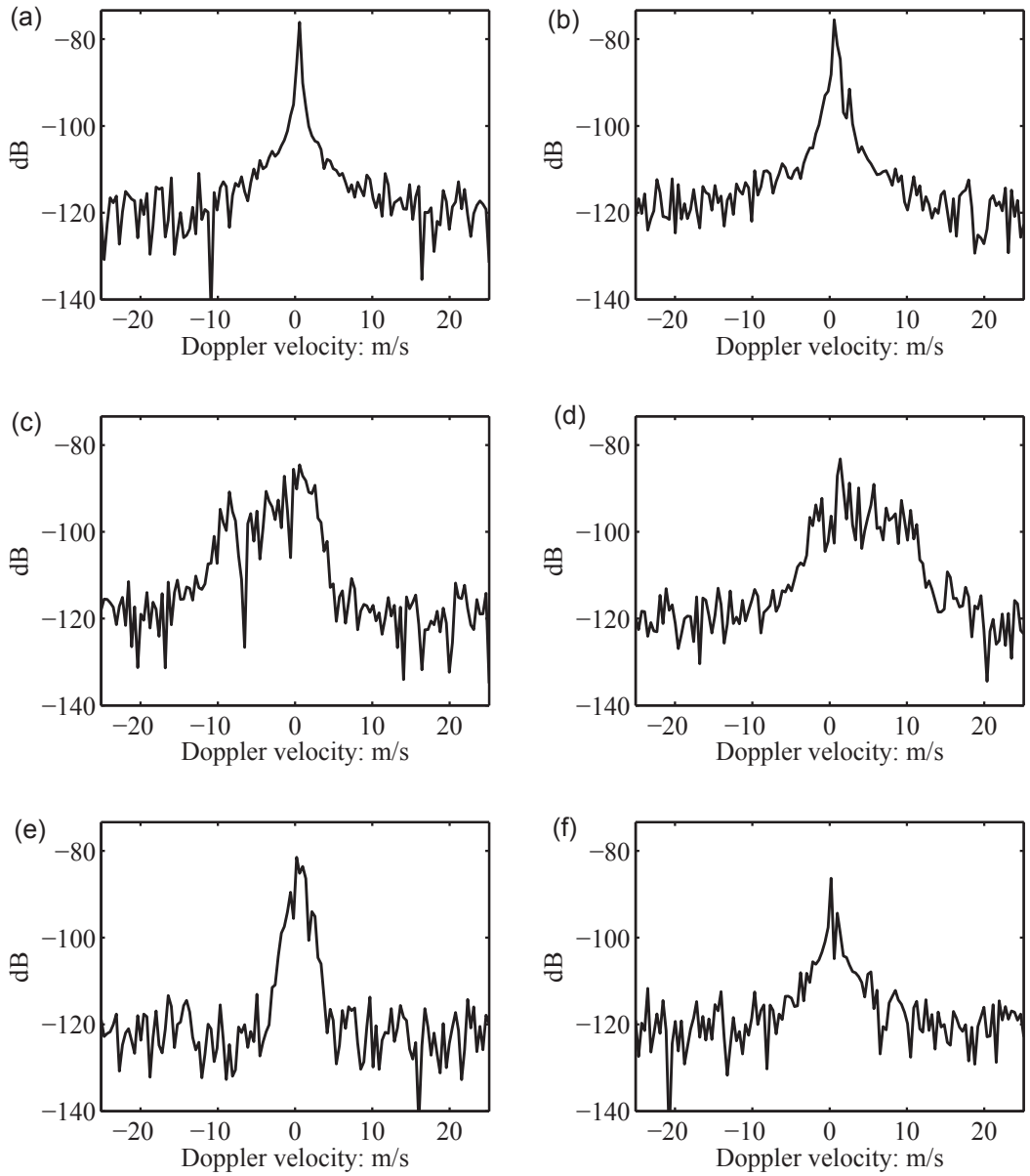

FIG. 12. X band Radar Doppler velocity spectrum of raindrops while vortex cores in two adjacent cells: (a) cell 01, (b) cell 02, (c) cell 03, (d) cell 04, (e) cell 05, (f) cell 06

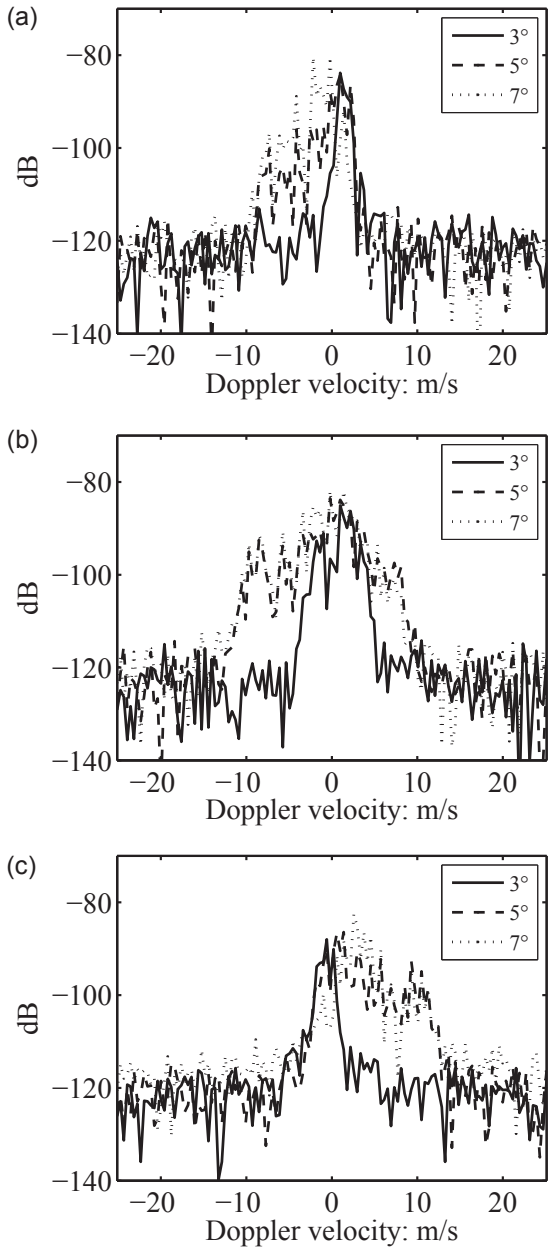

FIG. 13. X band Radar Doppler velocity spectrum of raindrops while vortex cores in two interval radar cells: (a) cell 02, (b) cell 03, (c) cell 04

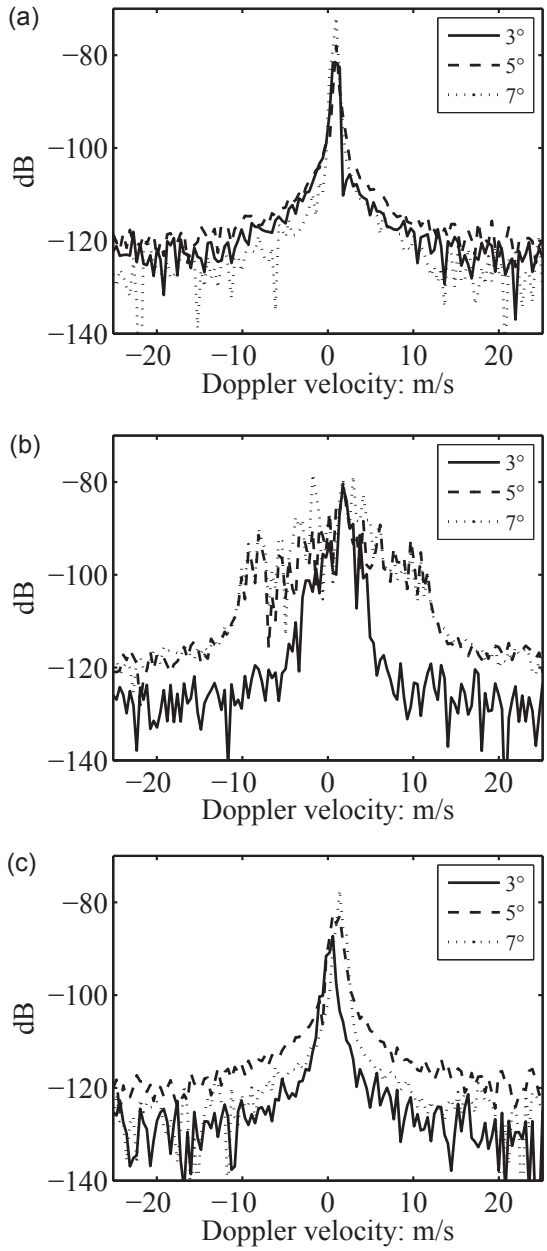

FIG. 14. X band Radar Doppler velocity spectrum of raindrops while vortex cores in the same radar cell with 100m range resolution: (a) cell 01, (b) cell 02, (c) cell 03

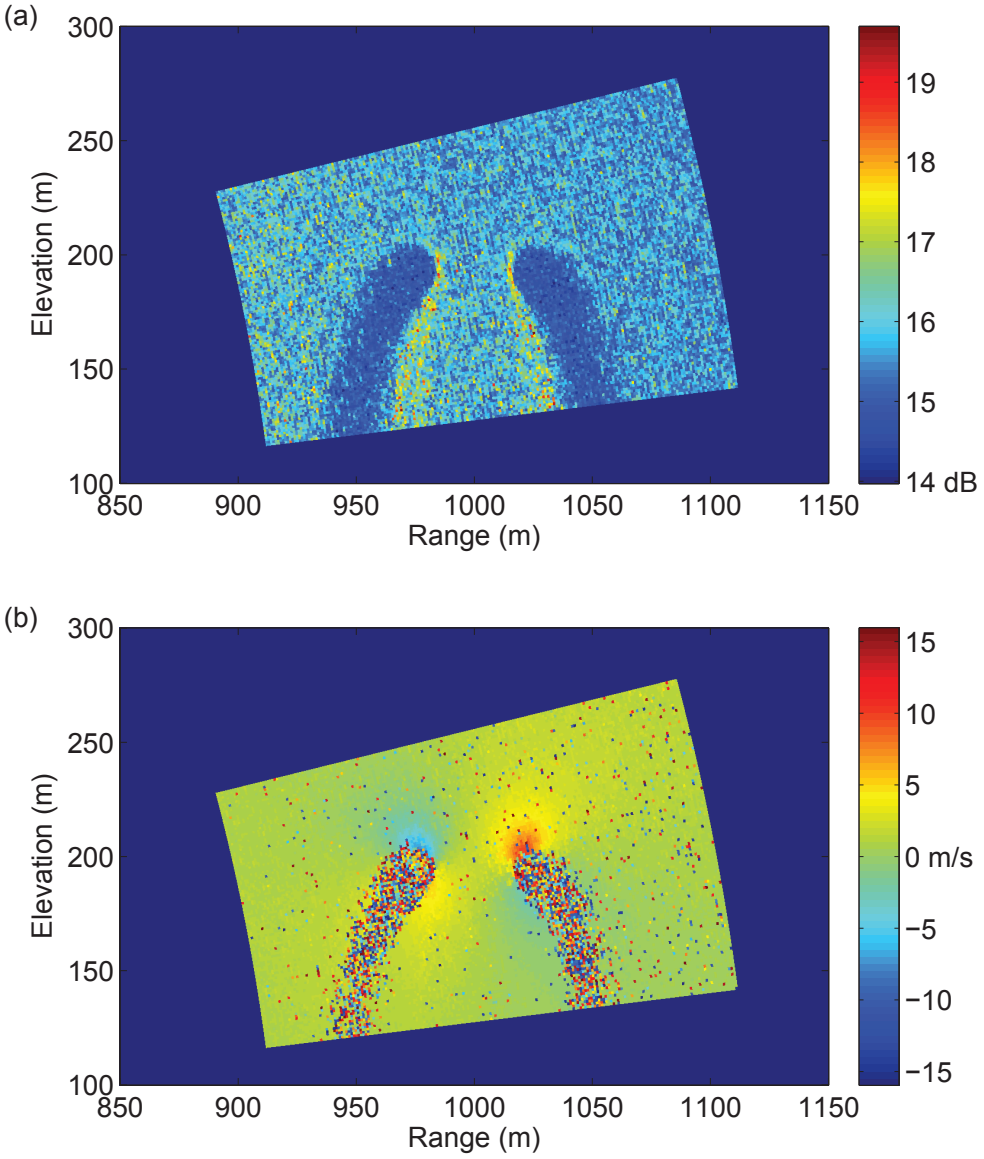

FIG. 15. W band radar signature of raindrops in wake vortices: (a)Average received power, (b)Retrieved Doppler velocity field